ELSEVIER

Microelectronics Journal 32 (2001) 959–967

Microelectronics Journal

www.elsevier.com/locate/mejo

Motion detection and stochastic resonance in noisy environments

G.P. Harmer*, D. Abbott

Centre for Biomedical Engineering (CBME) and Department of Electrical and Electronic Engineering, Adelaide University, Adelaide SA 5005, Australia

Received 15 June 2001; accepted 21 August 2001

Abstract

Several motion detection schemes are considered and their responses to noisy signals investigated. The schemes include the Reichardt correlation detector, shunting inhibition and the Horridge template model. These schemes are directionally selective and independent of the direction of change in contrast. They function by using spatial information and comparing it at successive time intervals. A rudimentary noise analysis is performed on the Reichardt and inhibition detectors to compare their natural robustness against noise. Using these detectors, stochastic resonance (SR) is applied, which is characterised by an improvement in response when noise is added to the input signal. It is found that the performance of the detectors degrades with the addition of noise. Employing Stocks' suprathreshold SR, an improvement can be gained when considering a network of detectors. Furthermore, when using an incorrect threshold setting for the template model, SR can be displayed.

Keywords: Smart sensors; Motion detection; Collision avoidance; Insect vision; Stochastic resonance; Noisy sensory neural models; Noise

1. Introduction

In poor weather conditions, millimetre waves offer a much greater penetration over the visible spectrum through small dust particles (aerosols), rain and fog. Antenna arrays capable of detecting mm-waves can be constructed [1]. This design utilizes radiometry, which is the science of using passive detection techniques to detect background radiation. Unlike radar, which transmits a signal then receives the backscattered radiation, a radiometer only receives naturally occurring blackbody radiation. It is reasonable to expect then, in this passive detection system, the signals are inherently noisy. Thus, the noise must be taken into account when processing the antenna array signals for the desired application.

The primary application is for a collision avoidance sensor, that is, a motion detector. This has stemmed from earlier work that developed a single 'seeing chip' [2–4] based on insect vision. This functioned in the visible spectrum and implemented a simple 'insect template model' to detect motion [5–7]. The aim is to extend this to the mm-wave spectrum and utilize the noise to develop a robust mm-wave collision avoidance sensor.

A common belief is that addition of noise to a system always degrades the quality of the response; however, by use of the phenomenon of stochastic resonance (SR), this is not always true. Certain non-linear systems have shown that there is an optimal non-zero noise intensity which can be added to a system to improve the response [8]. Originally developed for periodic signals, SR has been extended to systems with either sub or supra-threshold broadband (aperiodic) signals [9].

Three motion detection schemes have been investigated and we have evaluated the effects of SR in the presence of noisy signals. The first is the Reichardt detector, which was the earliest explicit model in motion processing [10]. The second involves shunting inhibitory neurons [11], which originated from a neurophysiological model [12]. The last is the Horridge template model, which is based on the navigation mechanism that bees use, to navigate [13]. This is included for historical reasons, and also because of its simplicity to implement.

2. Motion detection schemes

In order for a scheme to detect motion, in a directionally selective way, certain minimum requirements must be satisfied; asymmetry, two inputs and a non-linear interaction [14]. Two inputs are necessary since motion is a vector, a single receptor could not distinguish a change in intensity coming from either the left or right. A non-linear interaction between the inputs is required; otherwise, all information about the temporal sequence is lost. This inhibits the sensor

* Corresponding author. Tel.: +61-8-8303-6296; fax: +61-8-8303-4360.
E-mail addresses: gpharmer@eleceng.adelaide.edu.au (G.P. Harmer), dabbott@eleceng.adelaide.edu.au (D. Abbott).

0026-2692/01/$ - see front matter
PII: S0026-2692(01)00094-5

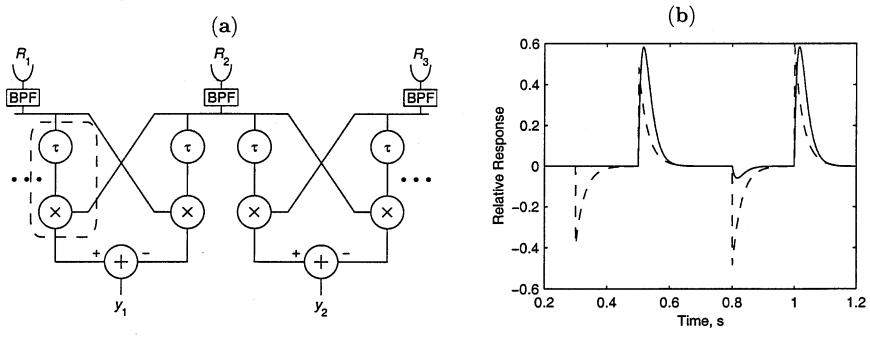

Fig. 1. (a) A section of the widefield Reichardt detector. (b)The response to two positive steps (0.5 and 1.0 s) with the BPF (solid line) and without (dashed line).

from being directionally sensitive. Finally, there must be some asymmetry between the two inputs; otherwise, the input receptors could be switched without affecting the output, giving no directional selectivity.

There are several broad categories of detection schemes, which stem from the basis of their conception. Biological schemes based on cellular mechanisms or neurophysiology can be divided into gradient and correlation type of models. Gradient schemes estimate motion by relating the changes in spatial and temporal intensity, whilst correlation schemes are essentially based on the common delay and compare systems. The other broad categories are the artificial schemes that take more engineering type of approaches.

Before going into details about the motion detection schemes, some criteria are established to determine the requirements of the schemes [11]:

- The sign of the response must indicate the direction of motion. This should be independent to the direction of change in contrast of the moving object.
- There should be no response to a stationary edge or a varying contrast.
- Ideally, it should be robust to noise.
- For an array of sensors, i.e. in the widefield, the position of the response should correspond to the moving edge. That is, spatially separated moving edges should each have a corresponding response.

The detectors that are considered in this paper are the Reichardt correlation detector, shunting inhibitory neuron and the Horridge template model.

2.1. Reichardt detector

Also called the correlation detector, it is one of the earliest biological motion detection systems based on the optomotor response of insects [10]. The Reichardt elementary motion detector (EMD) detects motion in one direction by comparing the signal from one receptor to a delayed signal from an adjacent receptor. The dashed box in Fig. 1(a) shows a single EMD. The comparison unit employs a simple multiplication, or correlation of the two signals. Due to the asymmetry of the EMD, there exists a preferred and a null direction. That is, the response to a stimulus moving in one direction has a larger magnitude (preferred direction) to the response of the same stimulus moving in the opposite direction (null direction). For the EMD highlighted in Fig. 1(a), the preferred direction is to the right and the null to the left.

Combining two EMDs tuned to opposite directions forms a bi-directional motion detector which is shown in Fig. 1(a) in the widefield configuration. Bandpass filters (BPF) are placed directly after the receptors to attenuate unwanted high frequency components in the response.

The delay stage, represented by τ, is modelled as an exponential decay, which is implemented as a first order low pass filter with the transfer function $H(s) = A/(s + A)$, where A is the cut-off frequency. This allows better integration of the delay stage into the biological modelling. The delay stage, along with the spatial separation of the receptors, allows tuning of the detector to different velocities.

The response of one of the local outputs (y_1 say) to a step input is shown in Fig. 1(b) by the solid line. This is briefly explained as follows. Consider a step with background luminance L that increases to $(1 + c)L$ whilst moving from left to right, where c is the contrast ($-1 \leq c \leq 1$). The output of the BPF is a pulse and with appropriate tuning, the delay time corresponds to the time taken to move between receptors allowing the pulses to coincide at the correlation unit to produce a positive response. The differencing of the EMDs then determines the sign of the direction. If the pulse generated by the BPF has not decayed before the stimulus reaches the next receptor, the pulse tail interacts causing a small dip.

This dashed line in Fig. 1(b) is the response of the Reichardt detector when the BPFs are omitted. The two peaks reveal the interactive mechanism at work, namely an excitatory one. This means that, every time a change is incident on one receptor, neighbouring outputs are affected, usually with the opposite magnitudes as seen in Fig. 1(b). Once the signals have been bandpass filtered, the effect of the excitatory mechanism is reduced to a small dip. This was

deliberately created by not allowing the tail from the BPF of the step input to decay away before the next step is incident. Hence, there is no dip in the first pulse in Fig. 1, but there is before the second pulse.

2.2. Inhibitory detector

Rather than using an excitatory mechanism to compare channels, an inhibitory mechanism is also capable of providing a directionally selective sensor. The first inhibitory mechanism proposed by Barlow and Levick was digital and was derived from studies of directionally selective units in rabbit's retina [12]. An alternative lateral inhibition mechanism, which resulted from studies of horseshoe crabs contains a linear interaction [15]. A non-linear version of this lateral inhibition, called *shunting inhibition* was developed by considering the neurochemistry of visual cells [16]. Using this type of neuron, motion detection systems that have similar behavioural properties to the Reichardt detector, have been developed [17]. The shunting inhibition neuron is described by the following non-linear equation

$$\frac{\mathrm{d}m}{\mathrm{d}t} = L - am - m\sum_i k_i f_i(X_i), \tag{1}$$

where $m(t)$ is the response (membrane voltage), $L(t)$ is the excitatory input, a is the self decay of the neuron, k_i are the weights, f_i are the activation functions and $X_i(t)$ are the inhibitory inputs. With regard to diagrams of the neuron, a dot represents the excitatory and a bar represents the inhibitory inputs, see Fig. 2 for example.

The modelling of the inhibitory neuron can be simplified by ignoring the internal dynamics, that is, setting $\dot{m} = 0$. This is equivalent to the steady-state operation and treats the neuron as a division operator giving

$$m = \frac{L}{a + \sum kf(X)}. \tag{2}$$

This simplifies the case studies when designing a detector based on this neuron, but in practice, it is highly susceptible to noise.

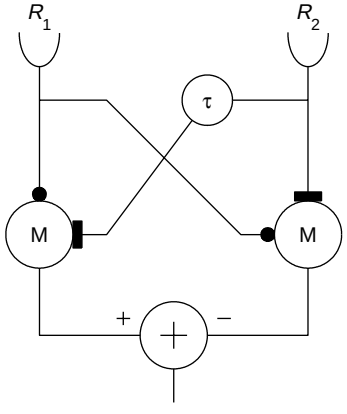

Fig. 2. Local inhibitory detector, M is the shunting inhibitory neuron.

The shunting neuron can be configured similar to the Reichardt detector, but the result does not satisfy the specified criteria — the response is dependent of the direction of contrast change. However, by constructing the inhibitory neuron as shown in Fig. 2, the problem is remedied. The difference is the excitatory input of both neurons is provided by the same receptor, the inhibitory inputs are provided by the other receptor. A delay inserted into one of the paths provides the asymmetry. A consequence of this is the response is zero until the stimulus reaches the inhibitory input. When the stimulus reaches the excitatory input (R_1), the output of both neurons change by the same amount which is cancelled at the summer. A response is only generated when the stimulus reaches the inhibitory input (R_2), since this contains the asymmetry. The overall effect of this configuration is the introduction of preferred and null directions that make it characteristically similar to the EMD.

Since the arrangement in Fig. 2 exhibits similar characteristic to the EMD, placing two back-to-back solves the problem of preferred and null directions and dependency on change of contrast. Since a response is only generated when the stimulus is incident on the inhibitory input coming from either direction, they are placed back-to-back centred about the inhibitory input. Such an arrangement is shown in Fig. 3 in the dashed box. This forms the directionally sensitive local inhibitory motion detector (DSLIMD) [11], with the response is given by y_i. The response y_i is also now independent to the direction of change of contrast.

In order to carry out a preliminary investigation of noise robustness, the Reichardt detector and DSLIMD with and without the internal dynamics, were subjected to the same

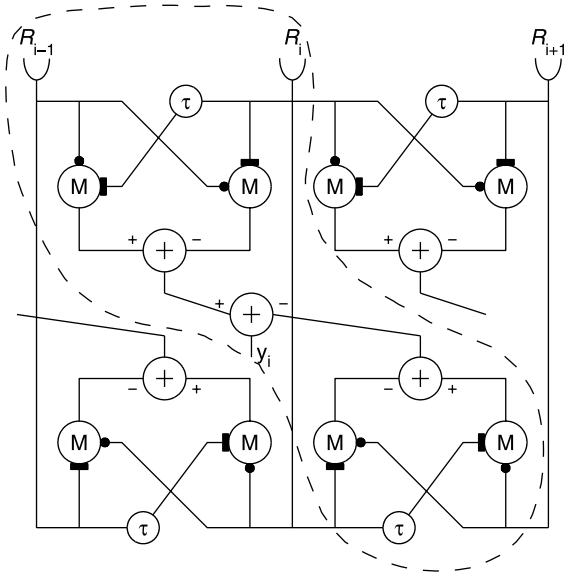

Fig. 3. The dashed outline shows a single slice of the DSLIMD from the widefield configuration. In practice, only one time delay element is required per receptor, two are drawn here for clarity.

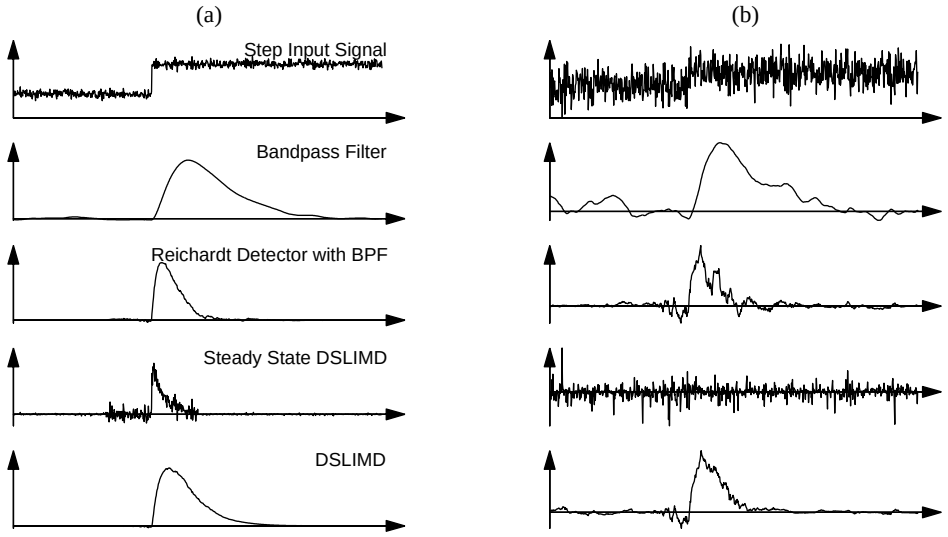

Fig. 4. Simple noise analysis. The horizontal axis of all plots is time over 0.8 s, the vertical axis of the top row is luminance (changing 10 to 12.5 levels of grey) and for the other rows it is a scaled response. Noise with standard deviation of 0.2 and 2.0 was added to column (a) and (b), respectively.

noisy signal. Although a bandpass filter does not satisfy the criteria for a motion detector, it is included to see how it modifies the input signals for the Reichardt detector and template model. The responses for small and large intensities of additive noise are shown in Fig. 4, they have been appropriately scaled for clarity.

One comparison immediately observable is the presence of internal dynamics is essential for robustness against noise. This includes the BPF, which can alternatively be expressed as a differential equation. This is in agreement with the response of the Reichardt detector without BPFs (not shown), which looks similar to the steady state DSLIMD. For the Reichardt and DSLIMD, the shapes are quite similar but the DSLIMD is not quite noisy.

2.3. Template model

The template model, originally developed by Horridge, to model insect vision, shares both biological and engineering heritage [13,18]. A diagram of the template model is shown in Fig. 5(a). The input channels are first bandpass filtered, which is then quantised by thresholding and sampling to give one of three states, increase (↑), decrease (↓) or no change (–). Templates are then formed by considering adjacent spatial channels at successive time intervals. This forms a 2×2 template that contains both spatial and temporal information to be used with a look up table. Since there are three possibilities for each of the four quadrants of the template, there are a total of 81 possible templates. By considering each of the possible templates,

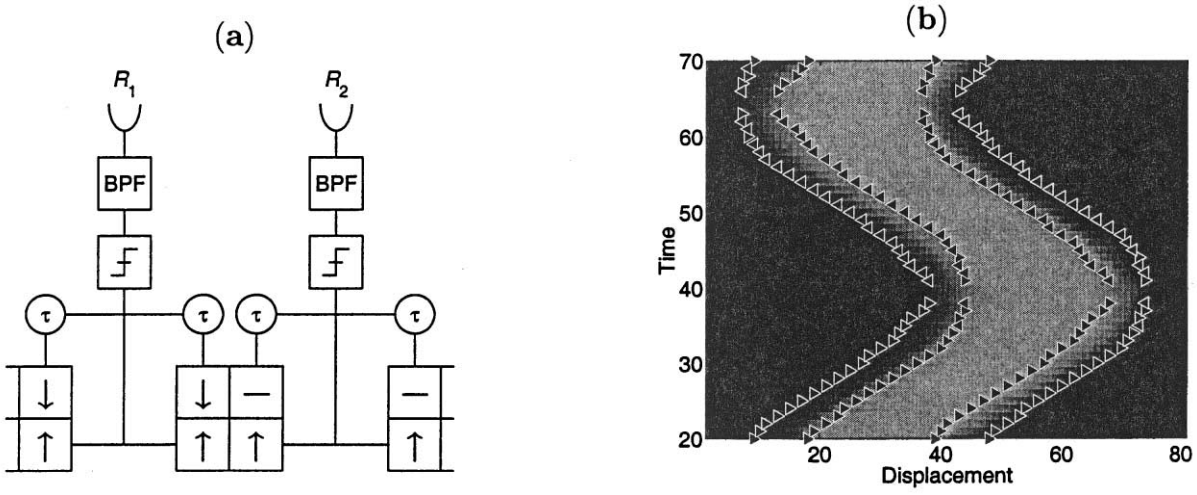

Fig. 5. Template model and response. (a) A section of the widefield schematic of the template model. The signal from the receptors is bandpass filtered, thresholded, sampled (not shown), delayed and stored as a 2×2 template. (b) The response to a step input being moved back and forth, ◁ and ▷ denote leftward and rightward motion, respectively.

only eight indicate coherent motion, which are known as directionally motion-selective templates (DMST) [5]. Although there are others that have the required 3:1 diagonal asymmetry [18] that indicate motion, the eight DMSTs used in this paper are those most immune to noise. By tracking particular templates, quantities such as velocity and time to impact can be calculated [6,7].

The response of the template model to a spot moving back and forth is shown in Fig. 5(b). This differs from the previous two schemes as the leading and lagging parts of the edge, not the edge itself is tracked [19]. Another difference is that it does not have any type of reliability measure, whereas for the previous schemes, larger response magnitudes indicated a higher probability of motion. The template model has a discrete output, either there is motion (left or right) or there is none, no matter how large the contrast difference is for example.

2.4. Performance measures

In communication systems, the performance of the detector can be easily quantified since its output should match the source as closely as possible. However, the output of motion detection schemes do not resemble that of the source (intensity images, for example); hence, some intermediate steps are necessary. The intuitive action is to create a benchmark, or some type of template from a clean signal. Mathematically, we can predict where the motion $M(x,t)$ is, from the instantaneous spatial and temporal gradients as

$$M(x,t) = \frac{\partial L}{\partial x}\frac{\partial L}{\partial t} = -L_{xt}, \tag{3}$$

where L is the luminance, x and t are space and time respectively. This provides a (change of) contrast independent measure of motion, the minus sign orientates a positive M as being rightward. Using this quantity as a benchmark, the performance of the motion detection schemes can be measured, via correlation or mean square error types of metric. It is important to use Eq. (3) only on clean images such as those generated by computer as differentiation operators are inherently noisy.

Eq. (3) is sufficient for the Reichardt and DSLIMD schemes, but it may not useful for the template model. This detects leading and lagging parts of an edge, thus we require a benchmark such as

$$\hat{M}(x,t) = \operatorname{sign}(M)|L_{xx}L_{tt}|. \tag{4}$$

To quantify the response, a normalised cross-correlation is taken with these quantities. This, along with an information theoretical measure is described in Section 3. A generalised network configuration is also described that will be used for the simulations.

3. Stochastic resonance

There are large amounts of literature relating to SR involving periodic signals (see Ref. [8] for an extensive review); thus, we will limit this discussion to the newer types of SR. They are aperiodic stochastic resonance (ASR) and suprathreshold stochastic resonance (SSR).

The term ASR, first coined by Collins [20,21] in 1995, describes a SR system that works with broadband signals. Clearly, the previous techniques using signal-to-noise ratio or modes in interspike interval histograms [22] are not appropriate for ASR. Collins et al. proposed a new measure, the power norm, with the normalised version given as

$$C_1 = \left\langle \frac{\overline{s(t)r(t)}}{\overline{[s(t)^2]}^{1/2}\overline{[(r(t)-\overline{r(t)})^2]}^{1/2}} \right\rangle \tag{5}$$

where $s(t)$ is the zero mean aperiodic signal and $r(t)$ is the response of the system. The overbar denotes an average over time and $\langle\cdot\rangle$, an ensemble average. Essentially, this is a simple input–output cross-correlation, as determined by the numerator, which is taken at a time lag of zero. In general, we wish to utilize the measure that quantifies the peak in the correlation function [21]. The two terms in the denominator are equivalent to the standard deviations of the signal and response, their purpose to normalise the correlation.

While ASR (and periodic SR) improves the response with the addition of noise, it lacks robustness due to the sensitive setting of the threshold. If the signal strength increases past the threshold, the addition of noise only serves to decrease C_1, which removes the SR from the system. It is shown that a much improved response can be gained by lowering the threshold so an output is always produced [23], although this requires a different system architecture. A promising alternative is SSR, where the signal is suprathreshold, with the threshold usually placed at the signal mean. This improves the robustness of the system, as the threshold setting is independent of the signal strength.

It has also been pointed out that one of the problems with using the measure C_1 is that it is a linear indicator based on linear response theory [24,25]. Although linearisation occurs for large enough amplitudes of noise [26], the system is designed primarily to be non-linear. Therefore, it seems inappropriate to use correlations, especially for small noise intensities. A more general indicator is the amount of information transmitted through a system, referred to as the average mutual information (AMI) [9]. In this setting, we consider a network of N devices, each with independent noise sources as shown in Fig. 6(a).

The Heaviside function forms one of the most simple non-linear devices and is described by

$$y(t) = \begin{cases} 1 & \text{if } x(t) + \eta_i(t) > \theta_i \\ 0 & \text{otherwise} \end{cases}, \tag{6}$$

where $\eta_i(t)$ are the noise and θ_i are the thresholds, $x(t)$ and $y(t)$ are the input and output, respectively. Thus, the response of the network is equal to the number of devices that have been triggered. Any model can be used in the

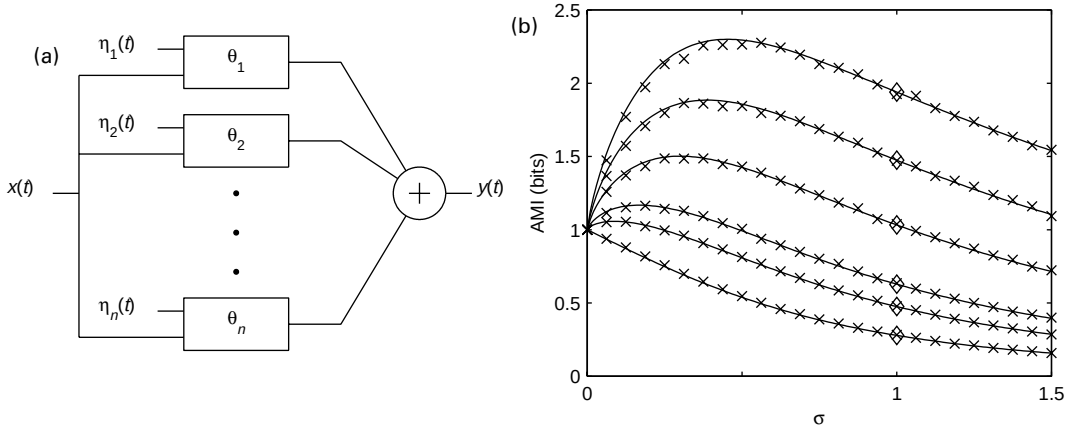

Fig. 6. (a) A summing network of N devices. (b) The AMI against the normalised noise $\sigma = \sigma_\eta/\sigma_x$ for various N with all $\theta_i = 0$, from bottom up the values of N are 1, 2, 3, 7, 15 and 31. The crosses are from simulations of the network and the lines are from numerically evaluating Eq. (7).

device usually some type of neuron model, but the Heaviside function is used for simplicity.

Having established the threshold network, the transmitted information is written as [9]

$$\mathrm{AMI} = H(y) - H(y|x) = -\sum_{n=0}^{N} P_y(n) \log P_y(n)$$

$$-\left(-\int_{-\infty}^{\infty} \sum_{n=0}^{\infty} P_x(x) P(n|x) \log P(n|x)\, \mathrm{d}x \right) \qquad (7)$$

where $H(y)$ is the information content (or entropy) of $y(t)$ and $H(y|x)$ is the amount of information lost in transmission. $P_y(n)$ is the probability the output $y(t)$ is n and $P(n|x)$ is the conditional probability density of the output being n, given the signal value x. The logarithms are taken as base 2, and thus the units of AMI are in bits. The AMI for several values of N (number of devices) are shown in Fig. 6(b), both from simulations of the system and numerically integrating Eq. (7). As mentioned earlier, an improvement due to SSR can be achieved for varying signal strength without modifying the threshold. This is true as long as the noise scales according to signal strength, which is highlighted by the x-axis of Fig. 6(b). This defines the noise intensity relative to the signal intensity as $\sigma = \sigma_\eta/\sigma_x$, where the σ's are the standard deviations of the respective signals.

It was pointed out by Stocks and colleagues that, placing all the thresholds at the same value is an inefficient use of N devices. Finding the set of optimal threshold, $\{\theta_i\}$, is a problem in 'optimal quantisation' where one must maximise the AMI [27]. Given that a system has a priori knowledge of the input signal, one can find the optimal threshold settings. For a uniformly distributed signal, uniformly distributing the thresholds between the limits of the signal leads to optimal threshold levels [25]. Note that the system is only optimal in the absence of noise, as the noise changes the distribution of the signal. The important result is that when noise is added to a system with optimal thresholds, it only proves detrimental to the system.

4. Simulations

The test sequences are based on what could be expected to be captured from a PC. A sample rate of 16 frames/second ($h = 1/16$) and an image width of 100–120 pixels was used. As mentioned earlier, the schemes process the horizontal lines of a 2-D image independently, which means that we only need to consider a vector image to gauge performance. Two test sequences were used, the first was simply a spot (intensities 10 and 12.5) moving back and forth with slightly blurred edges, similar to that shown in Fig. 5(b). The second consisted of a square wave grating (slightly blurred) with the same intensities moving in one direction for the first half of the time and the other direction for the last half of the time.

We first consider the Reichardt and DSLIMD configured in the network of Fig. 6(a). One can think of the widefield configuration shown in Fig. 3(a) being parallel with itself N times and the responses added to give the total response of the system. The correlation coefficient is calculated based on Eq. (5), taking into account the extra spatial dimension. The motion benchmark was generated using Eq. (3) from a noiseless image sequence. The delay between the input and output was compensated for, in order to produce the maximal input–output correlation.

It is easy to see from Fig. 7 that the addition of noise only degrades the response, the correlations generally decrease as the noise intensity increases, independent of the number of parallel detectors in the network. However, as we may intuitively expect, the performance improves as the number of elements in the network increase. This is due to the averaging properties of the Gaussian noise.

A possible explanation for the increased degradation of performance may be that the system is near optimal. In the

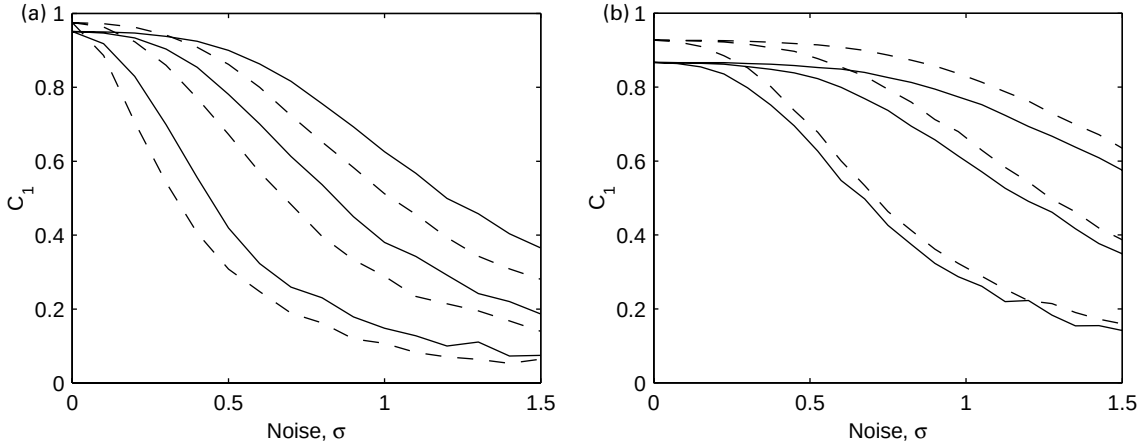

Fig. 7. Correlations for the (a) Reichardt detector and (b) DSLIMD versus the standard deviation of the added noise. The solid and dashed curves represent the single spot and grating stimulus, respectively and the number of elements in the network are 1, 8 and 32 from bottom to top.

absence of noise, the correlations are very close to unity with either high or low contrast images. The addition of noise does not add any more degrees of freedom to the system in the same way as the threshold network [24], thus no extra information is gained. Note, the correlation at zero noise depend on the input sequence and the parameters of the detector.

There are several ways to configure the template model in the parallel network due to the separable units it contains. We have considered two configurations, first, having the whole model in parallel in similar fashion to the previous detectors, or second, parallelising only the BPF and thresholding units. The first configuration is computationally more intensive as the template model must be formed in every device, whereas the second configuration only requires one template model formation.

Fig. 8 shows the correlations for both configurations of the template model. Since the outputs of the template model are spiky motion vectors, a short 2-D Hanning window is passed over the response. This is the technique used for finding the instantaneous firing rate from action potentials of neurons [21]. This simply smoothes the response to allow better matching to the motion benchmark, which is $\hat{M}$, in this case. The correlations shown in Fig. 8 have the threshold adjusted to best match the distance between the leading and lagging template to $\hat{M}$. In this situation, the addition of noise typically decreases the thresholds.

However, once the threshold is moved away from its optimal position (with respect to matching $\hat{M}$) definite SR characteristics are observed. This applies to both configurations of the template model, the latter is shown in Fig. 9. Recall that the placement of the threshold changes the spacing between template pairs, which may affect which benchmark to use, M or $\hat{M}$. The correlations for both have been shown in Fig. 9 to highlight this difference.

For a high threshold setting, the templates are close together and it also may be possible that no crossings are made for small noise intensities. The signal is subthreshold, thus we expect to observe classical SR, which is shown in Fig. 9.

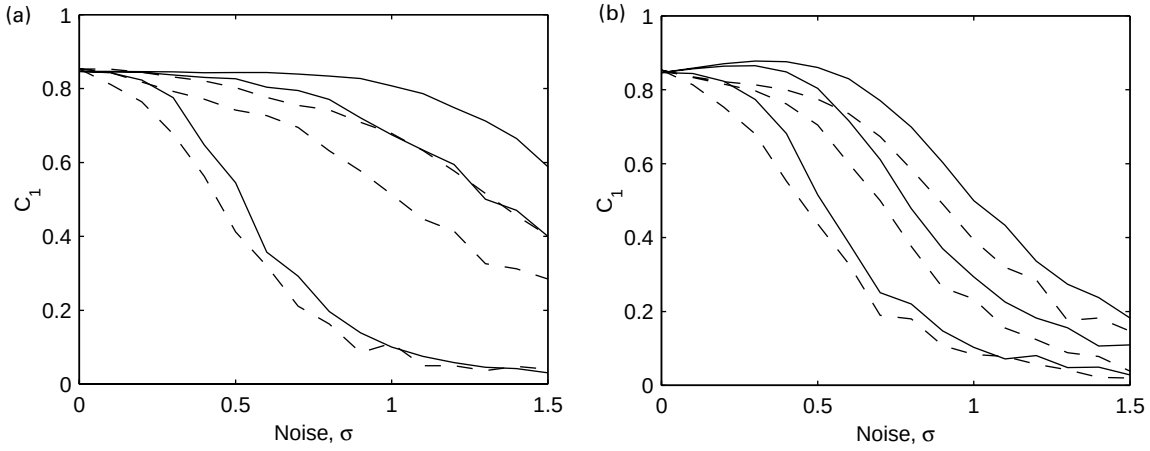

Fig. 8. Correlations for the template model. (a) BPF and threshold units in parallel. (b) Whole detector in parallel. The solid and dashed curves represent the single spot and grating stimulus, respectively and the number of elements in the network are 1, 8 and 32 from bottom to top.

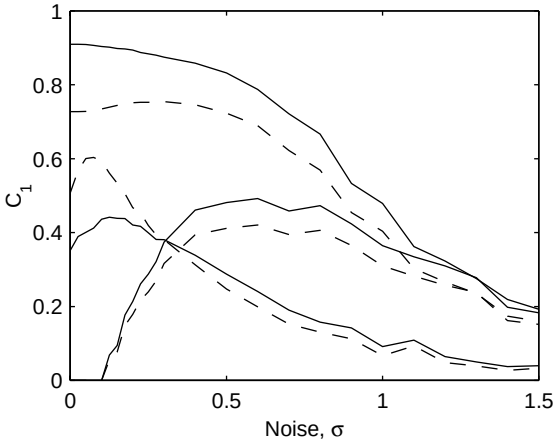

Fig. 9. Correlations for the template model (all in parallel) with $N = 16$. The solid and dashed curves represent correlations with M and $\hat{M}$, respectively and the pairs of curves from top to bottom have thresholds 0.1, 0.03 and 0.3, respectively.

For a low threshold setting the system is suprathreshold, that is, there is always a response even in the absence of noise. As expected, for a single detector, noise degrades performance (not shown). For more detectors in parallel, the performance actually improves until some optimal noise intensity is reached, whence the performance then continues to degrade as shown in Fig. 9.

This could prove useful if the contrast changes radically for some reason that makes the thresholds suboptimal. For example, if the lights are suddenly turned on or off, there is classical SR to provide for the small signal amplification and SSR to provide for the large signal amplification.

The improvement in correlations are due to the extra degrees of freedom that the noise adds to the system. In the absence of noise, the output of each detector is identical, thus the matching to M or $\hat{M}$ is not that good. The noiseless response produces sharp peaks, whereas the benchmark consists of wider, smooth curves. When a little noise is added, the motion vectors can deviate from this noiseless position a little, which gives more of a Gaussian spread to better match the benchmark. Hence, for low noise intensities, when the spread is small $\hat{M}$ is the better measure; but once the spreading becomes larger, the motion vectors tend to 'bunch up' making M a better measure. This explains why for low thresholds correlations with $\hat{M}$ start higher but die away quicker whereas with M they start low but are better in higher noise.

Though these image sequences exhibit stochastic resonant characteristics, it could be possible to find sequences that are optimally matched with no additional noise, in which case, noise only degrades the system. Similarly, we have only considered setting all the thresholds identically, which at least in a threshold network is an efficient use of the devices [27]. With the appropriate distribution of thresholds, noise may again be of no assistance.

5. Conclusion

The astute observer may note the qualitative results shown in Fig. 4 for $\sigma = 2.0$ appear better than the results in Fig. 7 for $N = 1$ at $\sigma = 2.0$. The reason is due to different parameter settings. Fig. 4 uses a much higher sampling rate ($h = 0.001$) and the generated pulse from the detector is spread over a longer time for demonstration purposes. In reality, we are only using $h = 1/16$ and we want the pulses to die down quickly before the next edge arrives. The tradeoff is that a shorter pulse width is more susceptible to noise, since we need to let higher frequency components through in the filter settings. These two factors dramatically diminish the robustness to noise, though the general trends are the same.

We have shown with these motion detection schemes using a simple network configuration, that no benefit is gained by adding noise to the signal when the system is operating optimally. However, departing from the optimal configuration in the template model, which contains a threshold function, noise can enhance the performance of the detector. Though when operating in the suprathreshold region, more than one device is required in the network. The detector performance is also improved by including more detectors in the network.

In a previous paper [28], the results for the template model did not show any benefit with the addition of noise. In [28], the template model was only used with the thresholds optimally set, thus as was shown in this paper noise only degrades performance. Furthermore, in this paper, the correlations for the template model have been normalised to provide a more reliable measure than the covariance (unnormalised correlation $\langle r(t)s(t)\rangle$). It is common for the covariance to monotonically decrease while the correlation coefficient can display SR [29], which is the case for some instances in the template model.

In this work, quantitative results were achieved via the use of correlations, which were based on Collins et al. original power norm C_1. Further work is required in order to implement an information theoretical measure. Another metric to consider is that of information transfer rate [30].

Acknowledgements

This work was funded by the Australian Research Council and the Sir Ross and Sir Keith Smith Fund.

References

[1] D.C. Goodfellow, G.P. Harmer, D. Abbott, Millimeter-wave collision avoidance sensors: future direfctions, Mobile Robots XIII and Intelligent Transportation Systems, Proceedings of SPIE, vol. 3525 1998 pp. 352–362.

[2] D. Abbott, A. Moini, A. Yakovleff, X.T. Nguyen, A. Blanksby, G. Kim, A. Bouzerdoum, R.E. Bogner, K. Eshraghian, A new VLSI

smart sensor for collision avoidance inspired by insect vision, Proceedings of SPIE, Boston, MA, vol. 2344 1994 pp. 105–115.
[3] D. Abbott, A. Moini, A. Yakovleff, X.T. Nguyen, R. Beare, W. Kim, A. Bouzerdoum, R.E. Bogner, K. Eshraghian, Status of recent developments in collision avoidance using motion detectors based on insect vision, Transportation Sensors and Controls: Collision Avoidance, Traffic Management, and ITS, A.C. Chachich, M.J.D. Vries (Eds.), Proceedings of SPIE 2902 (1997) 240–245.
[4] A. Moini, A. Bouzerdoum, K. Eshraghian, A. Yakovleff, X.T. Nguyen, A. Blanksby, R. Beare, D. Abbott, R.E. Bogner, An insect vision-based motion detection chip, IEEE Journal of Solid State Circuits 32 (2) (1997) 279–283.
[5] X.T. Nguyen, A. Bouzerdoum, R.E. Bogner, A. Moini, K. Eshraghian, Feature representation of motion trajectories, Proceedings of the IEEE International Conference of Neural Networks 6 (1995) 2922–2927.
[6] A. Yakovleff, A. Moini, From sensing to perceiving: an overview of the bugeye project, Advanced Focal Plane Arrays and Electronic Cameras, Berlin, Geermany 1996 pp. 86–96.
[7] R. Beare, A. Bouzerdoum, Two-dimensional motion computation using a template model, Proceedings of the International Conference on Systems, Analysis and Synthesis, Orlando, Florida (1996) 849–855.
[8] L. Gammaitoni, P. Hänggi, P. Jung, F. Marchesoni, Stochastic resonance, Reviews of Modern Physics 70 (1) (1998) 223–287.
[9] N.G. Stocks, Suprathreshold stochastic resonance in multilevel threshold systems, Physics Review Letters 84 (11) (2000) 2310–2313.
[10] W. Reichardt, Autocorrelation, a principle for the evaluation of sensory information by the central nervous system, in: W.A. Rosenblith (Ed.), Sensory Communication, Contributions to the Symposium on principles of sensory communication. The MIT Press, Endicott House, MIT, 1961, pp. 303–317.
[11] R. Beare, Image segmentation based on local motion detection, PhD Thesis, University of Adelaide, 1997.
[12] H.B. Barlow, W.R. Levick, The mechanism of directionally selective units in rabbit's retina, Journal of Physiology 178 (1965) 477–504.
[13] G.A. Horridge, A template theory to relate visual processing to digital circuitry, Proceedings of the Royal Society of London B 239 (1990) 17–33.
[14] A. Borst, M. Egelhaaf, Principles of visual motion detection, Trends in Neurosciences 12 (8) (1989) 297–306.
[15] H.K. Hartline, R. Ratliff, Studies in Excitation and Inhibition in the Retina, Rockefeller University Press, New York, 1974.
[16] R.B. Pinter, The electrophysiological bases for linear and for non-linear product term lateral inhibition and the consequences for wide field textured stimuli, Journal of Theoretical Biology 105 (1983) 233–243.
[17] A. Bouzerdoum, The elementary movement detection mechanism in insect vision, Philosophical Transactions of the Royal Society of London B 339 (1993) 375–384.
[18] G.A. Horridge, P. Sobey, An artificial seeing system copying insect vision, International Journal of Optoelectronics 6 (1/2) (1991) 177–193.
[19] X.T. Nguyen, Smart VLSI micro-sensors for velocity estimation inspired by insect vision, PhD Thesis, University of Adelaide, 1996.
[20] L.B. Kiss, Possible breakthrough: significant improvement of signal to noise ratio by stochastic resonance, in: R. Katz (Ed.), Chaotic, Fractal, and Non-linear Signal Processing, vol. 375, American Institute of Physics, Mystic, CT, 1996, pp. 382–396.
[21] J.J. Collins, C.C. Chow, T.T. Imhoff, Aperiodic stochastic resonance in excitable systems, Physical Review E 52 (4) (1995) 3321–3324.
[22] A.R. Bulsara, L. Gammaitoni, Tuning into noise, Physics Today 49 (3) (1996) 39–45.
[23] D.R. Chialvo, A. Longtin, J. Müller-Gerking, Stochastic resonance in models of neuronal ensembles, Physical Review E 55 (2) (1997) 1798–1808.
[24] N.G. Stocks, R. Mannella, Suprathreshold stochastic resonance in a neuronal network model: a possible strategy for sensory coding, in: N. Kosabov (Ed.), Future Directions for Intelligent Systems and Information Sciences, Physica, Wien, 2000, pp. 236–247.
[25] N.G. Stocks, Suprathreshold stochastic resonance, in: D.S. Broomhead, E. Luchinskaya, P. McClintock, T. Mullin (Eds.), Stochastic and Chaotic Dynamics in the Lakes, vol. 502, American Institute of Physics, Melville, NY, 2000, pp. 415–421.
[26] M.I. Dykman, D.G. Luchinsky, R. Mannella, P.V.E. McClintock, H.E. Short, N.D. Stein, N.G. Stocks, Noise-induced linearisation, Physics Letters A 193 (1994) 61–66.
[27] N.G. Stocks, Optimising information transmission in model neuronal ensembles, in: J.A. Freund, T. Poschel (Eds.), Stochastic Processing in Physics, Chemistry and Biology, Lecture Notes in Physics, vol. 557, Springer, Berlin, 2000, pp. 150–159.
[28] G.P. Harmer, D. Abbott, Smart sensor motion detection schemes in a noisy environment, Smart Materials and Sensors and MEMS, Proceeding of SPIE, Publisher, Melbourne, Australia 2001 pp. 25–35.
[29] N.G. Stocks, Private Communication, 2001.
[30] L.B. Kish, G.P. Harmer, D. Abbott, Information transfer rate of neurons: stochastic resonance of Shannon's information channel capacity, Fluctuation and Noise Letters 1 (1) (2001) L13–L19.